BNL-225164-2024-JAAM

GRP-COPD-11

Anti-Arrhenius behavior of electron transfer reactions in molecular dimers

N. Lin, T. Mani

To be published in "Chemical Science"

October 2023

Chemistry Department

Brookhaven National Laboratory

U.S. Department of Energy

USDOE Office of Science (SC), Basic Energy Sciences (BES)

DISCLAIMER

Anti-Arrhenius Behavior of Electron Transfer Reactions in Molecular Dimers

Neo Lin[1] and *Tomoyasu Mani*[1,2]*

[1] Department of Chemistry, University of Connecticut, Storrs CT 06269, United States

[2] Chemistry Division, Brookhaven National Laboratory, Upton NY 11973, United States

*tomoyasu.mani@uconn.edu / tmani@bnl.gov

ABSTRACT

Rates of chemical reactions typically accelerate as the temperature rises, following the Arrhenius law. However, electron transfer reactions may exhibit weak temperature dependence or counterintuitive behavior, known as anti-Arrhenius behavior, wherein reaction rates decrease as temperature increases. Solvent reorganization energy and torsion-induced changes in electronic couplings could contribute to this unusual behavior, but how each contributes to the overall temperature dependence is unclear. One can decelerate the charge recombination process in photogenerated radical pairs or charge-separated states by harnessing this often-overlooked phenomenon. This means that we could achieve long-lived radical pairs without relying on conventional cooling. Using a series of homo molecular dimers, we showed that the degree of

torsional hindrance dictates temperature-dependent torsion-induced changes in electronic couplings and, therefore, charge recombination rates. The overall temperature dependence is controlled by how changes in electronic coupling and the temperature-dependent solvent reorganization energy contribute to the rates of charge recombination. Our findings pave the way for rationally designing molecules that exhibit anti-Arrhenius behavior to slow down charge recombination, opening possibilities for applications in energy-related and quantum information technologies.

1. Introduction

The Arrhenius law[1]

$$k_{\mathrm{ET}} \propto \exp\left[\frac{-\Delta G^{\ddagger}(T)}{k_{\mathrm{B}}T}\right] \tag{1}$$

is a result of chemical kinetics, describes the temperature dependence of reaction rate constants, and is widely used as an empirical interpretation tool.[2] $\Delta G^{\ddagger}$ is the activation energy of the reaction. Electron transfer reactions typically follow the Arrhenius law. The nonadiabatic electron transfer equation (the Marcus equation)[3, 4] shows that the rate of electron transfer (k_{ET}) increases exponentially with increasing T:

$$k_{\mathrm{ET}} = \frac{2\pi}{\hbar}|V_{\mathrm{if}}|^2 \frac{1}{\sqrt{4\pi\lambda k_{\mathrm{B}}T}} \exp\left[-\frac{\left(\Delta G^0+\lambda\right)^2}{4\lambda k_{\mathrm{B}}T}\right] \tag{2a}$$

where V_{if}, λ, and ΔG^0 are the electronic coupling of the initial and final states, total reorganization energies, and the change in Gibbs energy. k_{B} and $\hbar$ are the Boltzman and reduced Planck constants. λ can have contributions from internal (λ_{V}) and solvent reorganizations (λ_{S}); $\lambda = \lambda_{\mathrm{V}} + \lambda_{\mathrm{S}}$. The activation energy is defined as

$$\Delta G^{\ddagger} = \frac{\left(\Delta G^0+\lambda\right)^2}{4\lambda} \tag{2b}$$

Rearrangement of eq. 2a shows that $\ln(k_{\mathrm{ET}}T^{1/2})$ has a linear (negative slope) relationship with the inverse temperature $1/T$.

$$\ln\left(k_{\mathrm{ET}}T^{\frac{1}{2}}\right) = \ln\left(\sqrt{\frac{\pi}{\hbar^2\lambda k_{\mathrm{B}}}}V_{if}^2\right) - \frac{\left(\Delta G^0+\lambda\right)^2}{4\lambda k_{\mathrm{B}}}\frac{1}{T} \tag{2c}$$

The linearity assumes that V_{if}, λ, and ΔG^0 are temperature independent. This linearity gives us experimental access to V_{if} and λ when ΔG^0 can be reasonably well determined or estimated. However, some key factors governing these parameters can be temperature-dependent: solvent reorganization energy (λ_{S}), ΔG^0 itself, and molecular conformations (associated V_{if}). Deviations from the temperature-dependent linearity of electron transfer reactions have been documented

but are scarce.[5] Slow solvent relaxation, most profoundly in glass-forming media,[6] can generally control the reaction rates to weaken the temperature dependence.[7] Electron transfer reactions in the Marcus inverted region could lead to very weak or almost no temperature dependence[8] because of the contributions from the high-frequency vibrational modes in the semiclassical Marcus equation, known as the Marcus-Jortner-Levich (MJL) equation (see **Supplementary Information** Section 2).[9-11]

The primary charge separation process in photosynthetic reaction centers exhibits an anti-Arrhenius behavior,[12] where k_{ET} decreases with increasing T. Bixon and Jortner attributed this unexpected behavior to the strong coupling to the medium vibrational motion modes.[13] Kim et al.[14] observed a bell-shaped temperature dependence, including anti-Arrhenius behavior, in *inter*molecular electron transfer reactions. Conformationally rigid molecular systems could offer more detailed insights. Using donor-bridge-acceptor (D-B-A) molecules, Davis, Ratner, and Wasielewski[15] later suggested that gating by torsional motion is responsible for such a counterintuitive behavior in *intra*molecular electron transfer reactions. Conformations of certain torsion angles can have stronger/weaker electronic couplings,[16] and therefore, a larger population of such conformations at higher temperatures could lead to acceleration/deceleration of electron transfer reactions. Their study suggested that long-distance electron transfer through longer oligo -phenylenevinylenes could exhibit more pronounced dependence on torsional motions because multiple linkages imparted more complex torsional motions. While torsional gating can control the rate of electron transfer reactions,[16-18] rigorous testing of its impact on temperature dependence, in particular anti-Arrhenius behavior, has been difficult because of the increasing complexity associated with D-B-A molecules such as multiple torsion angles among different units (e.g., oligo-*p*-phenylenevinylenes bridge) and energetic contributions. Specifically,

Matyushov and co-workers have elegantly shown that the temperature-dependent solvent reorganization energy[19] results in a bell-shaped dependence of k_{ET} on $1/T$; charge recombination rates decelerate at high and low temperatures.[20] Such temperature-dependence of solvent reorganization energy was also shown[21] to contribute to the very weak or almost no temperature dependence mentioned above.[8] Their results reaffirm the pronounced effects of reorganization energy in controlling electron transfer reactions while simultaneously casting the question of whether torsional motion could significantly contribute to the temperature dependence of electron transfer reactions, as suggested earlier. The effects of reorganization energies and torsion-induced changes in electronic couplings on rates of electron transfer reactions are illustrated in **Figure 1**. In the Marcus inverted region, a decrease of λ_S and smaller V can independently lead to slower k_{ET} at elevated temperatures at comparable ΔG^0.

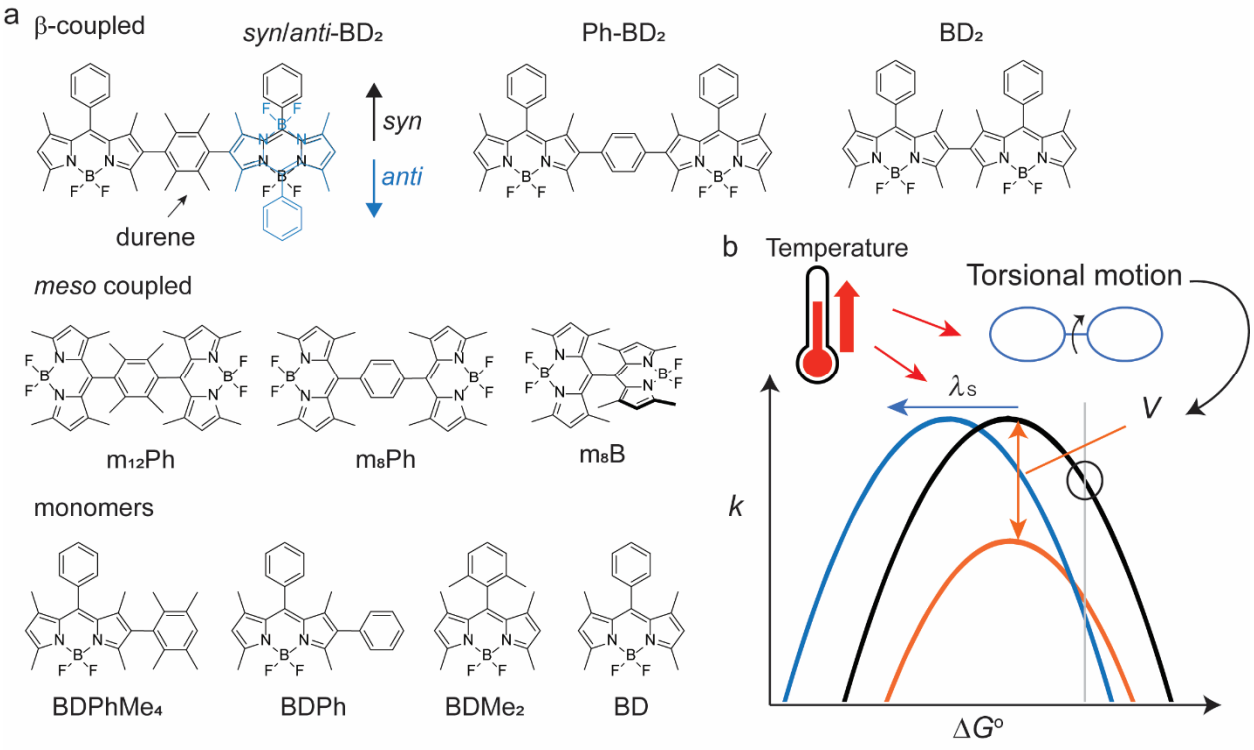

Figure 1. (a) Molecular structures investigated in this study. (b) Temperature can affect

electronic coupling (V) and solvent reorganization energies (λ_S) that could result in the anti-Arrhenius behaviors of nonradiative electron transfer reactions.

Long-lived radical pairs (RPs) or charge-separated states are critical for efficient charge generations in photovoltaics,[22] improving reactivity for photo-redox catalytic processes,[23] and better spin mixing and control of spin-correlated RPs for molecular quantum sensing,[24] communications, and computations.[25] While cooling is often used to achieve such long-lived states, we argue that anti-Arrhenius behaviors can be exploited as an alternative way of slowing down charge recombination, reducing the reliance on low-temperature/cryogenic environments. Here, we used a set of homo molecular dimers as a model system to further understand this underexplored behavior and showed that the change in torsional flexibility of single aryl moieties could result in the different temperature dependence in the solution phase and the observation of anti-Arrhenius behavior in charge recombination.

In homo molecular dimers, photoinduced electron transfer reactions are often symmetry-breaking charge separation (SBCS). SBCS has been the subject of extensive experimental and theoretical studies because of their crucial role in the light-harvesting reactions of center-specific chlorophyll molecules or "special pair".[26] Inspired by Nature's apparatus, many synthetic chromophores (dimers) and supramolecular assemblies have been designed to recreate SBCS, using polycyclic aromatic hydrocarbons and their derivatives[27-29] which include boron-dipyrromethene (BODIPY) chromophores.[30] BODIPY presents a unique opportunity where we can link two identical units at various locations,[31-36] allowing us to investigate the effects of torsional motions. Because of reduction potentials, some BODIPY dimers can undergo SBCS. Here, we use two distinct types of homo dimers; orthogonally (or *meso*-) coupled and β-β (here, simply β-) coupled dimers (**Figure 1a**). These two coupling sites provide different degrees of

flexibility in torsion angles without changing participating donor/acceptor molecular properties. We used unsubstituted benzene and a bulky counterpart, durene (1,2,4,5-tetramethylbenzene), as a bridge to further control torsional motions between the two BODIPY units. While two torsional motions do not necessarily move in sync, they are considered identical, given structural symmetry. Because of different potential energy surfaces (PES) along their respective torsion angles, the effect of "locking" of torsional motion by a bulky bridge is different for *meso*- and β-coupled dimers, making them exhibit different temperature-dependent electron transfer reactions and, therefore, allowing us to help understand the controlling factors of temperature dependence. Our findings suggest the possibility of rationally designing molecular systems whose charge recombination of photogenerated radical pairs exhibits anti-Arrhenius behavior.

The paper is organized as follows. We first describe the basic photo- and electrochemical characteristics of the new β-coupled BODIPY dimers (**Section 2.1-2.3**). Next, we present the study of photoinduced electron transfer reactions (symmetry-breaking charge separation and recombination) in the series of *meso*- and β-coupled BODIPY dimers at ambient temperature (**Section 2.4-2.5**). We then discuss the temperature-dependent photophysical properties, including anti-Arrhenius behaviors observed in both series (**Section 2.6**), followed by the conclusion (**Section 3**).

2. Results and Discussions

2.1. Synthesis and diastereomers of the β-coupled BODIPY dimers.

The synthetic scheme, procedures, and characterizations of the new molecules explored in this work are presented in **Supplementary Information** Section 1. In addition to the dimers with benzene and tetramethylbenzene as bridges, we prepared a direct β-β coupled dimer[37, 38] (BD_2, **Figure 1a**) for comparison. We also prepared the respective monomers as controls (BD, BDPh,

and $BDPhMe_4$, **Figure 1a**). The β-coupled dimer with a bulky bridge exhibits an interesting trait. Suzuki-Miyaura coupling of diiodotetramethylbenzene with mono-borylated BDs resulted in the formation of two stereoisomers of BODIPY dimers: the approximately centrosymmetric C_{2h} conformer (*syn*) and the C_{2v} non-centrosymmetric (*anti*) conformer. The polarities of these two conformers are significantly different from each other due to symmetry. The difference can be easily visualized by silica gel thin-layer chromatography (TLC) (**Figure 2a**), making it possible to isolate them using silica column chromatography and characterize them individually. Density functional theory (DFT) calculations support this large polarity difference (**Figure 2b**).

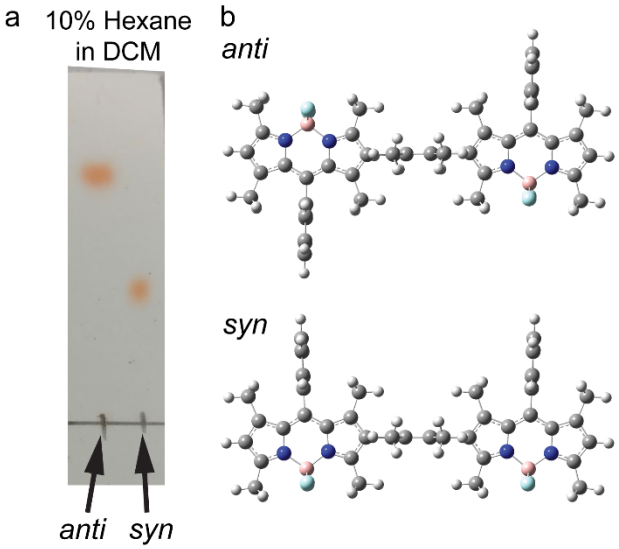

Figure 2. Stereoisomers of the β-coupled BODIPY dimers. (a) Visualizing the polarity difference of two conformers by silica gel TLC. (b) DFT optimized structures of *syn* and *anti*-BD_2 at B3LYP/6-31+g(d).

As the dipole moment of BODIPY is along the short axis,[39] the overall dipole moment becomes larger (μ ~ 10 Debye in the gas phase) in *syn*-BD_2 where the two BDs' short axis align in the same direction. On the other hand, the overall dipole moment of *anti*-BD_2 is much smaller (μ ~1 Debye), where the dipole moments of the two individual BDs align oppositely and cancel out

each other. Because it is highly nonpolar, the solubility of *anti*-BD_2 is poor in many organic solvents we tested, especially in polar solvents. While significantly different in polarity, the two stereoisomers (*syn*/*anti* diastereomers) behave almost identically within our experimental errors in the solution phase tested.

2.2. Photophysical properties of the β-coupled BODIPY dimers.

We recorded absorption and emission spectra in a select number of solvents. Normalized absorption and emission spectra of the dimers and corresponding monomers in chloroform are shown in **Figure 3**, and some photophysical properties are reported in **Table 1**.

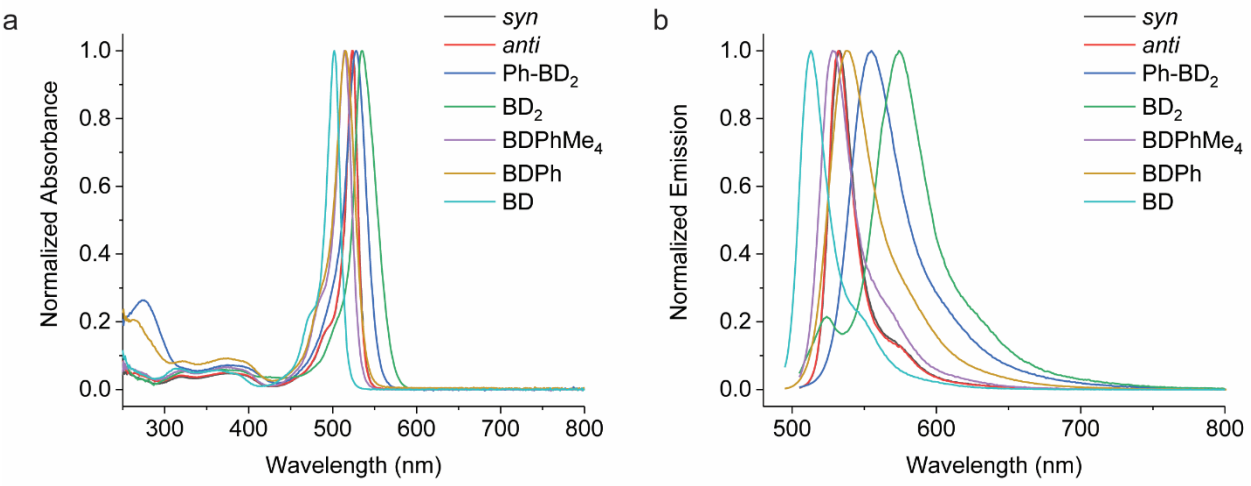

Figure 3. Steady-state photophysical characteristics of the β-coupled dimers and respective monomers in chloroform. (a) Normalized absorption spectra. (b) Normalized emission spectra (λ_{ex} = 480 nm).

The dimers' absorption and emission spectra are red-shifted compared to those of their respective monomers, and the degree of shifts varies from Ph-BD_2, *syn*/*anti*-BD_2, to BD_2. The shift of the emission peak relative to the absorption peak ($\Delta\nu = \nu_{em}^{max} - \nu_{abs}^{max}$) also depends on

the bridges of the dimers. These characteristics point to interesting exciton couplings. The exciton coupling is not the focus of this work, and we will present an in-depth analysis of these properties in a separate paper. The emission quantum yields of the dimers in chloroform (Φ_{em} ~ 0.8) are slightly higher than those of the corresponding monomers (Φ_{em} ~ 0.6-0.7). Emission lifetimes ($\tau = 1/k_{em}$) of the dimers are somewhat shorter than the corresponding monomers, but femtosecond transient absorption (fsTA) spectroscopy confirmed no significant additional nonradiative decay pathways (i.e., electron transfer reactions) for the dimers in chloroform (**Figure S1**). Among the dimers, Φ_{em} for *syn*/*anti*-BD_2 is higher than Ph-BD_2 and BD_2. Nonradiative decay constants (k_{nr}), calculated by $k_{nr} = (1 - \Phi_{em})k_{em}$, are smaller for *syn*/*anti*-BD_2 than the corresponding monomer ($BDPhMe_4$) and BD. This decrease in k_{nr} suggests that the improved rigidity imparted by durene, restricting rotations of both BD units, works in favor of increasing Φ_{em}.

Table 1. Select Photophysical Properties of the β-coupled BODIPY Dimers and Monomers in Chloroform.

	λ_{abs}^{max} (nm)	λ_{em}^{max} (nm)	$\Delta\nu$ [a] (cm^{-1})	Φ_{em}	τ (ns)	k_{rad} (s^{-1})	k_{nr} (s^{-1})
dimers							
syn-BD_2 (C_{2v})	523	532	359	0.83 ± 0.02	3.0	2.7×10^8	5.8×10^7
anti-BD_2 (C_{2h})	523	532	323	0.85 ± 0.02	3.0	2.9×10^8	4.9×10^7
Ph-BD_2	528	555	921	0.74 ± 0.02	3.2	2.3×10^8	8.2×10^7
BD_2	534	523, 574	1305	0.77 ± 0.02[b]	3.3[b]	2.6×10^8	7.6×10^7

monomers

BDPhMe4	514	528	516	0.73 ± 0.02	4.3	1.7×10^8	6.6×10^7
BDPh	515	538	830	0.74 ± 0.01	4.6	1.6×10^8	5.6×10^7
BD	502	513	427	0.61 ± 0.02	3.7	1.6×10^8	1.1×10^8

[a] $\Delta\nu = \nu_{\mathrm{em}}^{\max} - \nu_{\mathrm{abs}}^{\max}$. [b] The values are for the emission whose peak is at 574 nm.

We observed different and more complex emission properties of the dimers in a polar solvent, *N*, *N*-Dimethylformamide (DMF) (**Table 2**); notably, we observed significantly lower Φ_{em} and shorter emission lifetimes while those of the monomers are less affected by the change in polarity. They indicate that an additional deactivation pathway exists in the dimers in a polar environment: symmetry-breaking charge separation.

Table 2. Select Photophysical Properties of the β-coupled BODIPY Dimers and Monomers in DMF.

	$\lambda_{\mathrm{abs}}^{\max}$ (nm)	$\lambda_{\mathrm{em}}^{\max}$ (nm)	$\Delta\nu$[a] (cm^{-1})	Φ_{em}	τ (ns)	k_{rad} (s^{-1})	k_{nr} (s^{-1})
dimers							
syn-BD_2 (C_{2v})	521	531	252	0.13 ± 0.05	0.76	--	--
anti-BD_2 (C_{2h})	521	531	252	0.14 ± 0.05	0.76	--	--
Ph-BD_2	527	556	918	0.025 ± 0.02 (ex) 0.005 ± 0.02 (fl)[b]	0.16[c]	--	--
BD_2	534	573	1205	0.019 ± 0.02 (ex)	0.45s[c]	--	--

				0.016 ± 0.02 (fl)[b]			
monomers							
BDPhMe4	512	526	861	0.68 ± 0.02	4.0	1.7×10^8	8.1×10^7
BD-Ph	514	540	406	0.77 ± 0.02	4.7	1.6×10^8	4.8×10^7
BD	501	512	349	0.54 ± 0.02	3.6	1.5×10^8	1.3×10^8

[a] $\Delta\nu = \nu_{\mathrm{em}}^{\max} - \nu_{\mathrm{abs}}^{\max}$. [b] Φ_{em} (fl) is the emission quantum yield of the monomer-like BODIPY fluorescence, and Φ_{em} (ex) is the quantum yield of the BODIPY dimer excitons. [c] The reported values are based on the global fitting of time-resolved emission decays at multiple wavelengths. These values are NOT the lifetimes of "prompt" emission.

2.3. Electrochemical characterizations.

Electrochemical data show that the charge separation processes are energetically allowed in a polar solvent. We determined the reduction potentials by cyclic voltammetry (CV) in DMF, acetonitrile (MeCN), and dichloromethane (DCM), depending on the solubility of the compounds. The voltammograms of the β-coupled dimers and monomers in DMF are shown in **Figure S2**. The reduction potentials and associated data are reported in **Table 3** (DMF) and **Table S1** (MeCN and DCM). Details of the analysis of electrochemical data, including comproportionation constants, are given in **Supplementary Information**, Section 3.

Table 3. Reduction Potentials of the β- and *meso*-coupled BODIPY Dimers and Monomers[a]

	E_{red}^{1} [b] (●+/0, V)	E_{red}^{2} (0/●-, V)	E_{red}^{3} (●-/2-, V)	E_{red}^{4} [b] (2-/●3-, V)	E_{S1} (eV)	ΔG_{CS}^{0} [c] (eV)	ΔG_{CR}^{0} (eV)
β-coupled							
syn-BD2	0.70	-1.57		-2.52	2.36	-0.17	-2.19

anti-BD_2	0.73	-1.56		-2.81	2.36	-0.16	-2.20
Ph-BD_2[d]	0.70	-1.49		ND[e]	2.30	-0.19	-2.11
BD_2	0.76	-1.48	-1.66	-2.58	2.24	-0.14	-2.10
meso-coupled							
$m_{12}Ph$	0.70	-1.55	-1.64	ND[e]	2.45	-0.24	-2.21
m_8Ph[f]	0.81	-1.47	-1.50	ND[e]	2.44	-0.20	-2.24
monomers							
$BDPhMe_4$	0.68	-1.56		-2.49			
BDPh	0.70	-1.52		-2.44			
$BDMe_2$	0.70	-1.57		ND[e]			
BD	0.71	-1.56		-2.46			

[a] Reported vs. $Fc^{+/0}$ in DMF with 0.1 $TBA^+PF_6^-$ unless otherwise noted. The error is generally ± 0.02 V. [b] The peaks are irreversible, and the reported values are the peak value. [c] The reported values are for DMF. Determined by eq. 3. [d] We could not make reasonable measurements in DMF, and the values reported here are the estimations based on the data in DCM (**Table S1**) and scaled by the data of BDPh in DMF and DCM. [e] Not determined. [f] Reported vs. $Fc^{+/0}$ in MeCN with 0.1 $TBA^+PF_6^-$

We now consider the energetics of photophysical pathways in DMF (**Figure 4a**). We estimated the Gibbs energy change for charge separation by

$$\Delta G_{\mathrm{CS}}^{0} = e(E_{red}^{1} - E_{red}^{2}) - \frac{e^2}{4\pi\varepsilon_0\varepsilon_S r_{\mathrm{DA}}} - E_{00}^{\mathrm{S1}} \qquad (3)$$

where E_{red}^{1} and E_{red}^{2} correspond to the reduction of the radical cation and the neutral, respectively, and E_{00}^{S1} is the singlet excited state energy of the BODIPY dimer ([Dimer]* in **Figure 4a**), measured as the crossing point between the steady-state absorption and emission measured in DMF. The energies of the singlet excited state of the monomers (^{S}BD*, the "local" excited state) are slightly higher, and excitation at a shorter wavelength results in the population

of the monomer excited state in DMF. We estimated r_{DA} as a center-to-center distance based on DFT-optimized structures; r_{DA} = 12.5 Å for *syn*/*anti*-BD_2, Ph-BD_2, and r_{DA} = 8.4 Å for BD_2. The estimated ΔG^0_{CS} are negative in all the dimers, showing that we have a large enough driving force of charge separation, and SBCS is energetically allowed in DMF.

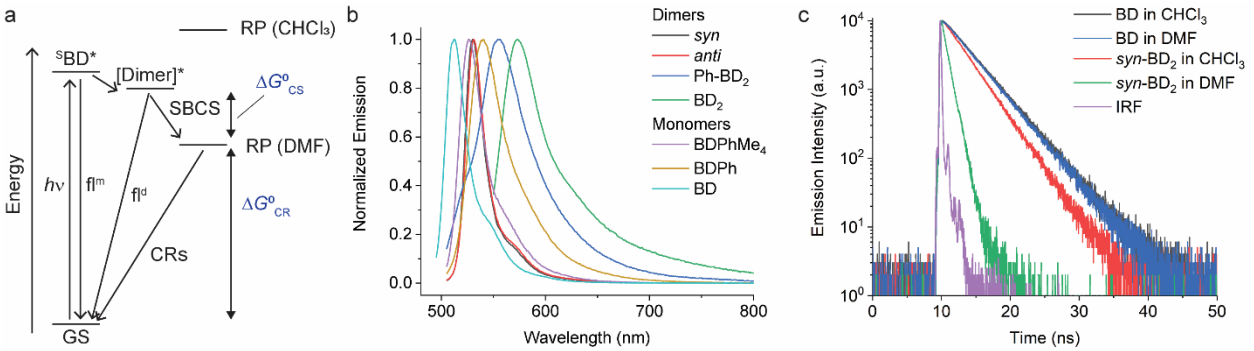

Figure 4. Overview of the photophysical pathways of the β-coupled dimers. (a) Photophysical diagrams of the dimers. The energy scale is arbitrary. Triplet excited states are not shown for brevity. (b) Emission spectra of the β-coupled BODIY dimers (λ_{ex} = 540 nm for BD_2 and 490 nm for the rest). (c) Comparison of BD and *syn*-BD_2 emission lifetimes in chloroform and DMF (λ_{ex} = 506 nm).

2.4. Symmetry-breaking charge separation in the β-coupled dimers.

We observed SBCS for all the β-coupled dimers. The observations are similar to the *meso*-coupled dimers reported by Thompson, Bradforth, and co-workers (e.g., m_8Ph and m_8B, **Figure 1**).[30] In this section and the following (Sections 2.4 and 2.5), we focus on the effect of torsional degrees of freedom on charge separation and recombination. As part of the study, we also introduced 1,2,4,5-tetramethylbenzene in the *meso*-coupled dimers (m_{12}Ph, **Figure 1a**, named after ref [30]) and compared the effects of a bulky bridge on these dimers.

The first evidence of SBCS in the β-coupled dimers comes from emission measurements, as briefly mentioned above. Absorption and emission spectra of all the dimers in DMF are shown in **Figure S3** and **Figure 4b**, respectively. The absorption spectra are similar to those in chloroform except for small blue shifts in peak wavelengths (**Table 2**). On the other hand, we observed some changes in emission properties. One indication of SBCS is the low quantum yield of emission. The quantum yields of the dimers in DMF are significantly smaller than those in chloroform (see **Table 1** for chloroform and **Table 2** for DMF). For example, Φ_{em} of *syn*-BD_2 is 0.83 and 0.13 in chloroform and DMF, respectively. We observed only one emission peak for *syn*/*anti*-BD_2, which looks more like the BD local emission. For Ph-BD_2 and BD_2, we observed BD local and exciton [Dimer]* emissions, and their Φ_{em} is reported separately. Emission lifetime measurements showed a monophasic decay for *syn*/*anti*-BD_2 and biphasic decay for Ph-BD_2 and BD_2, where the faster component is dominant (~ 90%). The monophasic decay for *syn*/*anti*-BD_2 is faster than the corresponding monomers in both DMF and chloroform (**Figure 4c**). They also correspond to the excited state/RP decays determined by fsTA spectroscopy (see below). The faster components of the biphasic decays for Ph-BD_2 and BD_2 agree with the rate of charge recombination determined by fsTA (see below). The slower component of the biphasic decay may be due to the monomer-like emission that might come from populations that do not undergo electron transfer reactions or slight impurities. We did not capture the "prompt" dimer exciton/local BD excited state emission decays that can reflect the rates of SBCS. Those decays in Ph-BD_2 and BD_2 are faster than the time-resolution of our TCSPC setup (~20-30 ps) as shown by fsTA, and therefore we could not determine the lifetime of these emissions.

To gain further insights into time-resolved photophysical behaviors in these dimers, we performed fsTA spectroscopy. We used global fitting to analyze each fsTA data set with a

sequential, irreversible, kinetic model (A → B → C→⋯). The spectral profiles obtained from analysis with a sequential scheme are called evolution-associated decay spectra (EADS).[40] The EADS of *syn*-BD_2 in DMF are presented in **Figure 5a,** and those of Ph-BD_2 and BD_2 are presented in **Figure S4**.

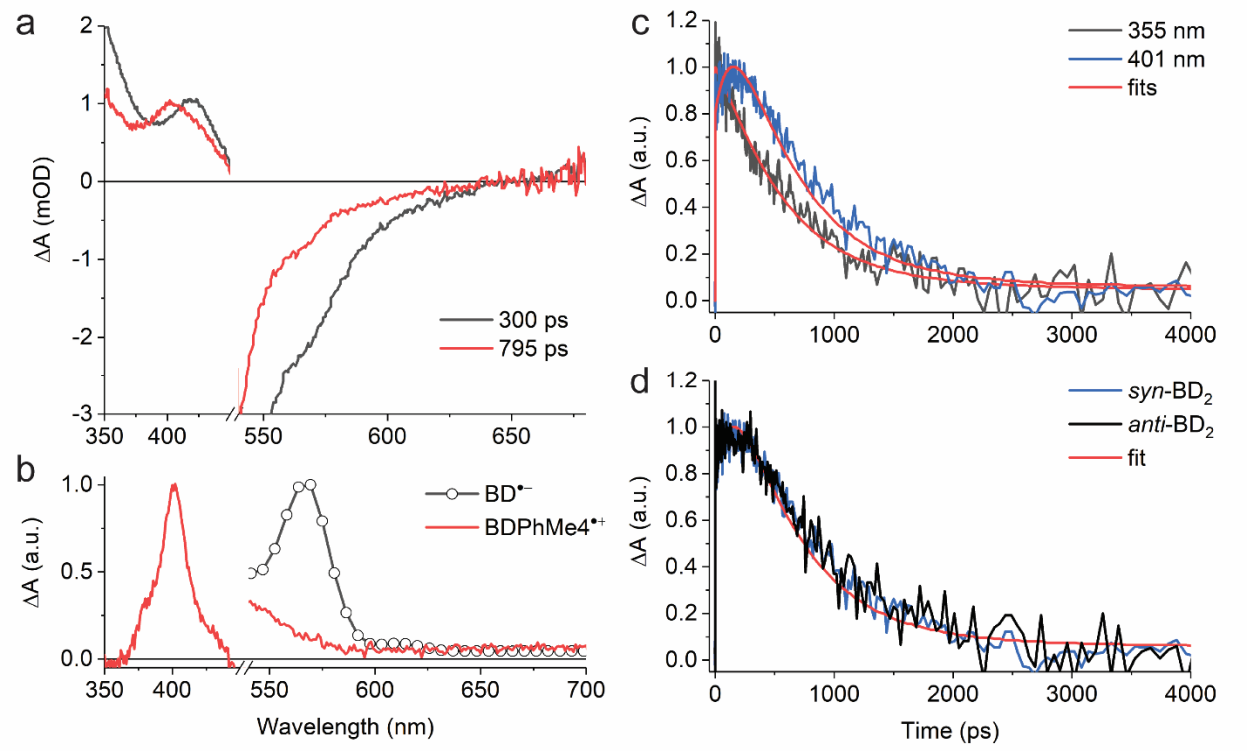

Figure 5. Photoexcitations of s*yn*- and *anti*-BD_2 result in the formation of RPs in DMF. (a) EADS of *syn*-BD_2 with corresponding lifetimes upon photoexcitation at λ_{ex} = 500 nm. (b) The absorption of radiolytically generated radical anions of $BD^{\bullet-}$[41] and electrochemically generated $BDPhMe4^{\bullet+}$. (c) Decay kinetics of *syn*-BD_2 at 355 and 401 nm in DMF upon photoexcitation at λ_{ex} = 500 nm. (d) Comparison of the decay kinetics of s*yn*- and *anti*-BD_2 at 401 nm in DMF upon photoexcitation at λ_{ex} = 500 nm.

Although we could identify a component that has the spectral signature of $BD^{\bullet-}$ (~560 nm[41]) in the single value decomposition (SVD)'s components in all the β-coupled dimers data set in DMF, the features are not clear in the EADS likely because of the overlap with the ground state bleaching. On the other hand, we observed the absorption peak at ~400 nm in EADS (e.g., EADS with τ = 800 ps for *syn*-BD_2) that agrees well with the absorption band of BODIPY radical cations ($BDPhMe_4^{\bullet+}$) that we recorded spectroelectrochemically (**Figure 5b**). The rise times of this peak at ~400 nm (**Figure 5c**) correspond to k_{SBCS} obtained by global fitting: note that $k_{SBCS} >> k_{S1}$ in the absence of SBCS. Consistent with the emission measurements, the TA measurements showed identical (within experimental errors) photophysical pathways for *syn* and *anti*-BD_2; representative kinetic traces are shown in **Figure 5d,** and rate constants are reported in **Table 4**. Again, no electron transfer reactions were observed in less polar solvents like chloroform and toluene: fsTA data of *syn*-BD_2 in chloroform are presented in **Figure S1**.

Table 4. Kinetic Rates for Transitions between the Excited States of the β- and *meso*-connected BODIPY Dimers at Room Temperature in a Polar Solvent.

	Solvent	$1/k_{SBCS}$ (ps)	$1/k_{CR}$ (ps)		$1/(k_{fl}+k_{nr})$ (ps)[b]
			fsTA [a]	Emission [b]	
β-coupled					
syn-BD_2	DMF	300 ± 20	800 ± 20	--	760 ± 20 [c]
anti-BD_2	DMF	300 ± 20	790 ± 20	--	760 ± 20 [c]
Ph-BD_2	DMF	17 ± 8	126 ± 18	150 ± 20 [d]	
BD_2	DMF	7 ± 1	340 ± 25	450 ± 20 [d]	
meso-coupled					
$m_{12}Ph$	DMF	180 ± 10	1070 ± 100	--	

m_8Ph	DMF	60 ± 10	260 ± 50	--	
	MeCN[d]	50 ± 10	200 ± 80		
m_8B	MeCN[d]	0.8 ± 0.2	2000 ± 100		
monomers					
BDPhMe$_4$	DMF				4060 ± 100
BDPh	DMF				4790 ± 100
BD	DMF				3630 ± 100

[a] Determined by transient absorption spectroscopy. [b] Determined by time-resolved emission measurements. [c] The decays are monophasic. [d] The decays are biphasic, and the short component corresponds to k_{CR} (see Table 2). [e] Data were taken from ref [30].

Based on the TA spectra at a longer time scale, we determined that the production of triplet excited states of BDs in these dimers in DMF are negligible, meaning triplet productions by neither spin-orbit charge-transfer (SOCT-ISC)[41-45] nor radical pair intersystem crossing (RP-ISC) followed by triplet charge recombination is efficient in the current systems. Therefore, we can exclude the spin effects on the charge recombination rates.

2.5. Effects of tetramethylbenzene in β- and *meso*-coupled dimers.

All the dimers follow the photophysical pathway depicted in **Figure 4a** with varying rate constants. Charge separation (k_{SBCS}) becomes slower, but recombination (k_{CR}) becomes faster for Ph-BD$_2$ than a more compact BD$_2$. This somewhat unexpected observation of faster charge recombination at a shorter distance is similar to the *meso*-coupled BODIPY homo dimers previously reported (m_8Ph vs. m_8B where m_8Ph has benzene between two BODIPYs, see **Figure 1** for the structure and rate constants for **Table 2**) though the effect in the β-coupled dimer case is smaller. Thompson, Bradforth, and co-workers used this observation to support the hypothesis

that molecules with higher torsional rigidity exhibit longer charge-separated state lifetimes (slower k_{CR}) because of a higher barrier to reaching resonance between the ground and CS surfaces.[30] This set of our data supports this hypothesis. In contrast to Ph-BD_2 and BD_2, the two BODIPY planes of *syn*/*anti*-BD_2 are more "locked" to a coplanar configuration because of structural hindrance by tetramethylbenzene as shown by the PES scanned along the torsion angle (φ). The comparisons of PES for BD_2, BDPh, and $BDPhMe_4$ are shown in **Figure S5**. k_{SBCS} is about 15 and 40 times slower for *syn*/*anti*-BD_2 than for the unconstrained counterpart Ph-BD_2 and the more compact BD_2, respectively. The effect is comparably smaller for the recombination process because k_{CR} is only about 2 and 6 times slower for *syn*/*anti*-BD_2 than for Ph-BD_2 and BD_2, respectively. The trends on SBCS and CR are depicted in **Figure 6a**, **b**.

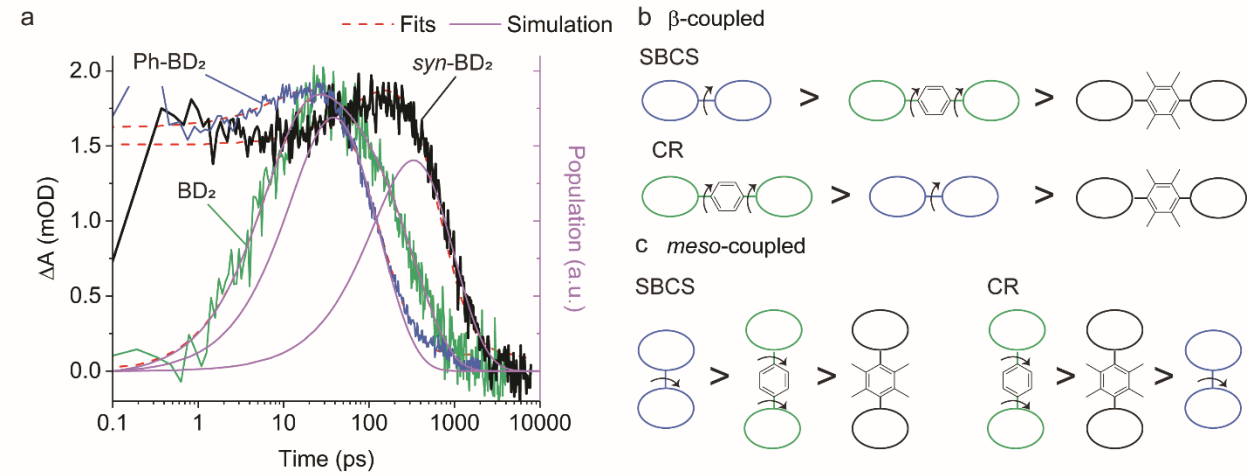

Figure 6. Tetramethylbenzene slows down charge separation and recombination of the β- and *meso*-coupled BODIPY dimers. (a) CS state population as a function of time for the β-coupled dimers: *syn*-BD_2, Ph-BD_2, BD_2. Transient absorption (TA) signals (left y-axis) and population (right y-axis) taken from simulations of SBCS are overlayed. TA signals are measured at 401, 396, and 400 nm for *syn*-BD_2 (black line), Ph-BD_2 (blue line), and BD_2 (green line). Note that the early times of the TA signal of *syn*-BD_2 and Ph-BD_2 overlap from the initial excitons. (b) The

pictorial representations of the observed trends of the rates of SBCS and CR among the β-coupled and (c) *meso*-coupled BODIPY dimers. The circles represent BODIPY moieties. The arrows represent torsional motions.

To further examine the effect of the structural hindrance by tetramethylbenzene, we prepared a structurally constrained *meso*-coupled BODIPY dimer (m_{12}Ph, **Figure 1**). We also prepared m_8Ph for comparison. The steady-state absorption and emission spectra of m_8Ph and m_{12}Ph in DMF are reported in **Figure S6.** The synthetic scheme, characterization, and basic photophysical characterizations in chloroform and DMF are reported in **Supplementary Information** Experimental Section, **Table S2**, and **Table S3**, respectively. The voltammograms and electrochemical data are reported in **Figure S7** and **Table 3**. The Gibbs energy change of charge separation (ΔG^0_{CS}) for m_{12}Ph and m_8Ph are also reported in **Table 3**, using eq. 3 with r_{DA} = 8.8 Å.[29] We performed fsTA measurements in DMF, and EADS of m_{12}Ph and m_8Ph are presented in **Figure S8,** in which we could clearly identify the spectral signatures of both the BODIPY radical cation and anions. Interestingly, introducing tetramethylbenzene slowed down SBCS but did not significantly elongate the RP lifetime (**Table 4**). m_8Ph behaves very similarly in DMF and MeCN (**Table 4**), and we can fairly compare the rate constants with the data set of m_8B recorded in MeCN.[30] k_{CR} is ~3.5 times slower in m_{12}Ph than m_8Ph, but 2 times faster than the more compact m_8B. SBCS and charge recombination are still the fastest and slowest in m_8B among the three *meso*-coupled dimers, respectively, as illustrated in **Figure 6c**, further signifying the large structural reorganization required for charge recombination in m_8B.[30] The differences in the effect of tetramethylbenzene on the photophysics between the β- and *meso*-coupled BODIPY dimers reflect the more pronounced change of conformational restrictions imposed by

tetramethylbenezene in the β-coupled dimers. The PES along the phenyl ring's torsion angle (φ) in the β and *meso*-coupled dimers showed more flexibility at the β position. We discussed the PES data in the context of temperature dependence in **Section 2.6**. One interesting observation is the difference in the degree of electronic couplings, judged by the transfer integrals, for electron and hole between the β- and *meso*-coupled dimers: $t_H > t_E$ for the β-coupled dimer and $t_E > t_H$ for the *meso*-coupled dimer. This difference reflects how atomic orbitals contribute to the HOMO and LUMO of BODIPY. For LUMO, a significant contribution comes from the carbon at the *meso* position but not from the carbon at the β position. In contrast, for HOMO, more contribution comes from the carbon at the β position (**Figure S9**). These differences may indicate that the charge separation occurs through electron transfer for the *meso*-coupled dimers and hole transfer for the β-coupled dimers. Other details of the PES are presented in **Supplementary Information** Section 4.

2.6. Temperature dependence of electron transfer reactions in the dimers.

Temperature-dependent measurements show the different anti-Arrhenius behaviors for the charge recombination processes in the β- and *meso*-coupled dimers series. Here, we focus only on two pairs of β- and *meso*-coupled dimers with a bridge.

First, SBCS follows the expected Arrhenius behavior for all four molecules (**Figure 7a, b**). We can fit the data with eq. 2c, assuming that λ, electronic coupling between the S1 and RP states (V^*), and ΔG^0_{CS} are temperature independent. In the fitting, λ and V^* are variables while we keep ΔG^0_{CS} = -0.17 and -0.16 eV for *syn*-BD_2 and Ph-BD_2 and -0.24 and -0.20 eV for m_{12}Ph and m_8Ph as reported in **Table 3**.

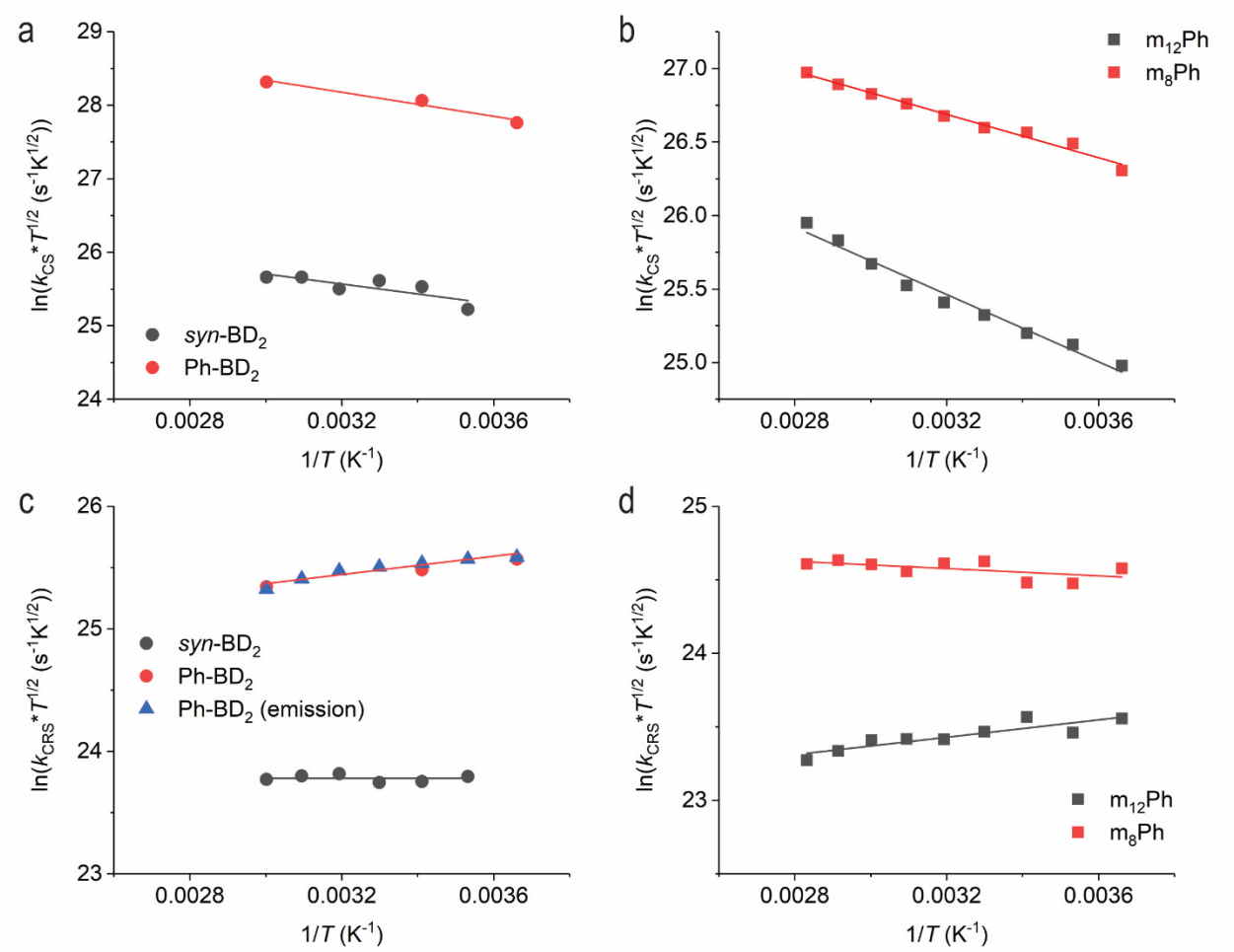

Figure 7. Temperature-dependent charge separation of (a) the β-coupled and (b) *meso*-coupled BODIPY dimers. Temperature-dependent charge recombination of (c) the β-coupled and (d) *meso*-coupled BODIPY dimers. The data are from fsTA measurements unless otherwise noted in the legend. The lines are fitted lines to eq. 2c.

Expectedly, SBCS occurs in the Marcus normal region. Given the relatively fast rates of SBCS, the reaction is expected to occur from the excited states at the nuclear of the ground states (Franck-Condon states), and solvent reorganization energies may not change significantly over the temperature range. The obtained V^* are about the same in the *meso*-coupled dimers, while the structurally unconstrained dimer, Ph-BD2, is about 4-5 times larger than the structurally

constrained dimer *syn*-BD_2. The fitted parameters (λ and V*) for all four dimers are reported in **Table S4**. The difference in the coupling is consistent with the PES data (**Figure 8**, and **Supplementary Information** Section 4) that showed that the energy minima are the same for the two *meso*-coupled dimers (m_8Ph and $m_{12}Ph$) while it shifts to that of lower electronic coupling (hence slower charge separation) for a structurally constrained *syn*-BD_2 compared to Ph-BD_2.

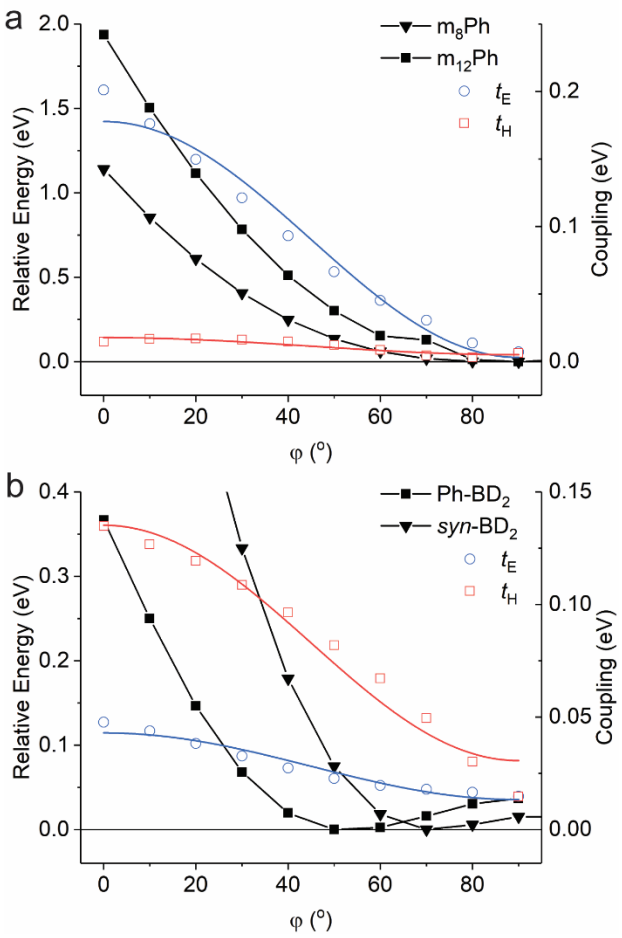

Figure 8. Potential energy surfaces for (a) the *meso*-coupled and (b) β-coupled BODIPY dimers as a function of torsion angle (φ). The couplings are reported as the transfer integral of electron and hole (t_E and t_H). The coupling data are fitted with equation $V = V_0\, cos^2(\varphi) + V_a$. V_0 and V_a

describe the coupling constants where one torsion angle is at φ = 0° and φ = 90°, respectively, while the other is at the optimized configuration.

Charge recombination processes do not follow the expected Arrhenius behavior. Temperature-dependent fsTA measurements directly monitor charge recombination and show that charge recombination rates of the unconstrained Ph-BD_2 slowed dramatically at elevated temperatures. For example, $1/k_{CR}$ of Ph-BD_2 is 136 ± 10 ps at T = 0 °C, which slowed to 68 ± 10 ps at T = 60 °C. The charge recombination processes, determined by fsTA, are almost temperature-independent for *syn*/*anti*-BD_2 (**Figure 7c**). As noted above, the measured emission lifetime for the β-coupled Ph-BD_2 corresponds to the charge recombination of RPs, which showed the same trend. From T = 0 °C to 60 °C, we observed an increase in exciton emission lifetime, and the nonradiative charge recombination rates slowed by ~40 % (**Figure S10**). The emission lifetime of *syn*-BD_2 is not temperature-dependent (**Figure S11**). In clear contrast, we observed the anti-Arrhenius behavior for the constrained *meso*-coupled dimer m_{12}Ph, but the charge recombination was almost temperature-independent for the unconstrained counterpart m_8Ph (**Figure 7d**). While the emission lifetimes do not directly reflect the charge recombination for the *meso*-coupled dimers, the recombination fluorescence lifetime of m_{12}Ph increases as temperature increases while m_8Ph decreases (**Figure S12**).

The fits of the CR data to eq. 2c gave us near zero to negative activation energies (positive slopes, **Figure 7c**, **d**). We could also not fit the data even with the MJL equation when we assumed ΔG^0_{CR}, λ_S, and V_{if} are temperature-independent (see **Supplementary Information** Section 2 for details). Given the structural similarity, the nature of the resulting charges within RPs is similar among the four molecules, especially among the two of the same series. Indeed,

the electrochemical measurements show the almost identical ΔG^0_{CR} (**Table 2**). Therefore, the observed difference in the temperature dependence of the charge recombination rates must come from the structural factors associated with the bridge moieties (i.e., torsional motion).

We first look at the most structurally constrained m$_{12}$Ph. The torsion angle minimum between the BD core and phenyl ring in the *meso*-position is φ = 90º. Please see **Figure 8a** for the PES for the dimers and **Figure S13** for the control BODIPYs. The introduction of tetramethylbenzene in the *meso*-position does not alter the optimal φ from m$_8$Ph to m$_{12}$Ph, while it further restricts the motion with extra methyl groups locking the torsion angle more to the orthogonal configuration for m$_{12}$Ph. This locking significantly raises the energy barrier to access "flatter" conformations of higher electronic couplings. We can consider m$_{12}$Ph as one extreme case of "strong" torsional hindrance with a single minimum at the orthogonal configuration along 180º rotation.[46] Given this steep potential barrier present in m$_{12}$Ph, little structural changes occur along the torsion angle over the temperature range of our study, keeping the electronic coupling constant. This structural rigidity is corroborated by the fact that the nonradiative decay of the control BODIPY (BDMe$_2$, **Figure 1a**) is almost temperature independent, compared to the usual increase in nonradiative decay with an increase in temperature for BD (**Figure S14**). The phenyl rotation at the *meso*-position is responsible for the increased nonradiative decay.[47, 48] Their radiative decays are temperature-independent (**Figure S14**).

Therefore, we can attribute this temperature-dependent change in k_{CR} of m$_{12}$Ph to temperature-dependent solvent reorganization energies. Fitting the data to the MJL equation showed a decrease in λ_S as temperature increases. The fitting details are presented in **Supplementary Information** Section 2. In short, we fitted the data with temperature-dependent λ_S and ΔG^0_{CR} while V_{if} was assumed to be temperature independent (see above). This decrease in λ_S at higher

temperatures is consistent with the earlier experimental observations by Zimmt and co-workers[49, 50] and the models by Matyushov.[19, 20] The obtained electronic coupling is similar to V^* obtained from the fitting of the CS data (V_{if} = 25 cm^{-1} vs. V^* = 30 cm^{-1}).

As the solvent reorganization energies primarily come from the solvation surrounding the charged species, this recombination rate change with λ_S occurs for m$_8$Ph as well. On top of this contribution from the temperature change in λ_S, we have a contribution from torsional change. Because of the shallower potential barrier, m$_8$Ph can adopt "flatter" configurations of higher electronic couplings at higher temperatures, which are more favorable for charge recombination. This torsion-induced change in electronic couplings counteracts the change with λ_S, making the overall trend almost temperature-independent. Indeed, we can fit the more or less temperature-independent k_{CR} data of m$_8$Ph to the MJL equation by assuming a temperature-dependent V_{if} (**Supplementary Information** Section 2). The obtained V_{if} for m$_8$Ph (44 cm^{-1} at T = 20 °C) is higher than that for m$_{12}$Ph, corroborating more flexible torsional motion and hence a higher coupling for m$_8$Ph.

We now turn our attention to the β-coupled dimers. For the structurally unconstrained Ph-BD$_2$, the energy minimum is at the configuration of an intermediate electronic coupling (**Figure 8b**). We can classify Ph-BD$_2$ as a "weak" torsional hindrance case.[46] As the energy barrier toward the orthogonal configuration is much shallower compared to the barrier toward the "flatter" configurations, it will more likely take conformations of lower electronic couplings at higher temperatures. Coupled with the underlying change in λ_S, this torsion-induced change in electronic coupling slows down the charge recombination process at higher temperatures, leading to the observed anti-Arrhenius behavior. On the other hand, the tetramethylbenzene bridge fixes the phenylene ring to be more orthogonal to the BODIPY planes (φ ~70° for *syn*-BD$_2$ vs. ~ 50°

for Ph-BD_2) and lowers the energy barrier for the orthogonal configuration ($\varphi \sim 90^o$) significantly; $\Delta E = E$ ($\varphi = 90^o$) - E (optimal φ) = 15 meV vs 37 meV for *syn*-BD_2 and Ph-BD_2. At the same time, it raises the energy barrier for "flatter" configurations, compared to Ph-BD_2. The energy minima of *syn*-BD_2 are therefore more orthogonal, and we can also classify *syn*-BD_2 as a "strong" torsional hindrance case.[46] Yet, compared to the *meso*-coupled counterpart ($m_{12}Ph$), the torsional motion is not as severely restricted (**Figure 8**). Note that the energy scale (y-axis in **Figure 8** and **Figure S13**) is about five times larger for the *meso*-coupled dimers (**Figure 8a**), signifying the existence of more severe torsional rigidity compared to the β-coupled dimers (**Figure 8b**). Therefore, at elevated temperatures, *syn*-BD_2 can still take conformations of higher electronic couplings and, consequently, favor charge recombination. This increase in electronic coupling counteracts the change in λ_S to have almost temperature-independent charge recombination for Ph-BD_2 over the temperature range of our study in a similar manner to m_8Ph.

3. Conclusions

While the Arrhenius law bears significant importance in chemistry, anti-Arrhenius behavior remains an underexplored phenomenon. Here, we investigated the role of torsional motion and solvent reorganization energy in the temperature dependence of the photoinduced symmetry-breaking charge separation and recombination reactions. As part of the study, we prepared a new series of β- and *meso*-coupled BODIPY homo dimers with 1,2,4,5-tetramethylbenzene as a bulky bridge. Because of the structural rigidity, we could identify and isolate the two stereoisomers for the β-coupled dimers (*syn*- and *anti*-BD_2). The photophysical and electrochemical characterizations showed almost identical behaviors of these two stereoisomers in the solution phase we tested. Tetramethylbenzene as a bridge reduces the electronic coupling and, therefore,

slows down the electron transfer processes in both β- and *meso*-coupled BODIPY dimers compared to the dimers with an unsubstituted phenyl bridge, but the extent of reduction differs.

Temperature-dependent measurements revealed that both series of dimers exhibit anti-Arrhenius behaviors in the charge recombination process. The two series of homo dimers capture the two different cases of torsional hindrance usually observed: strong and weak. In a *meso*-coupled dimer, restricted torsional motion favors the conformation of the least electronic coupling (strong torsional hindrance). The severe restriction imposed by tetramethylbenzene does not allow the constrained dimer (m_{12}Ph) to take conformations of higher electronic couplings even at elevated temperatures, effectively keeping the coupling constant fixed at the minimum over the tested temperature range. Yet, the change in solvent reorganization energy leads to anti-Arrhenius behavior in charge recombination. The unconstrained *meso*-coupled dimer (m_8Ph) can take conformations favorable for electron transfer reactions at elevated temperatures due to a shallower energy barrier. This results in counteracting the contribution from the solvent reorganization energy and, overall, in almost temperature-independent charge recombination processes. On the other hand, because of a weaker torsional hindrance, the unconstrained β-coupled dimer (Ph-BD_2) takes the conformation with intermediate electronic coupling. Temperature increase shifts it to take conformations of lower electronic coupling ($\varphi \sim 90^{o}$) which are unfavorable for electron transfer reactions, resulting in the anti-Arrhenius behavior. On the other hand, the constrained β-coupled dimers (*syn*/*anti*-BD_2) can take the conformations of (close to) the least electronic couplings due to the structural hindrance. The elevated temperature shifts the equilibrium to conformations of higher electronic coupling and, therefore, faster electron transfer reactions. This change in couplings counteracts the solvent

reorganization energy contribution to have the overall charge recombination trend temperature independent.

While the temperature dependence of solvent reorganization energy, when present, leads to anti-Arrhenius behavior of electron transfer reactions under a certain temperature range,[20] we demonstrate that a simple torsional motion can significantly modify the temperature dependence. The nature of modifications depends on the strength of torsional hindrance, and we can synthetically control such a hindrance to exhibit anti-Arrhenius behavior (e.g., m_{12}Ph in DMF). The current study shows that we can rationally design the molecular systems to take advantage of this underexplored chemical phenomenon to decelerate charge recombination of SCRPs without cooling down. This strategy may be helpful in producing long-lived SCRPs for energy- and quantum information technologies.

Data availability

All relevant data are available from the corresponding author upon reasonable request.

Author contributions

L. N. – investigation, writing, T. M. – conceptualization, project administration, funding acquisition, investigation, writing.

Conflicts of interest

There are no conflicts to declare.

Footnote. Electronic supplementary information (ESI) available.

Experimental methods, characterizations of new compounds, fitting details, electrochemical studies, discussions on PES, Figures S1-14, Tables S1-4, additional reference, and NMR data.

Acknowledgements

The authors acknowledge funding by the National Science Foundation under Grant No. 2144787, an NSF CAREER Award. The computational studies were performed at the cluster located in the Chemistry Division of the Brookhaven National Laboratory through work funded by LDRD 23-030. We thank Mr. Miu Tsuji and Mr. Michael Vrionides for synthesizing m_8Ph and $BDMe_2$, respectively, and Dr. Dariusz Niedzwiedzki for providing us with ASUfit 3.0 software.

REFERENCES

1. S. Arrhenius, Über die Reaktionsgeschwindigkeit bei der Inversion von Rohrzucker durch Säuren, *Z. Phys. Chem.*, 1889, **4U**, 226-248.
2. B. Peters, Common Features of Extraordinary Rate Theories, *J. Phys. Chem. B*, 2015, **119**, 6349-6356.
3. R. A. Marcus, On the Theory of Oxidation-Reduction Reactions Involving Electron Transfer .1., *J. Chem. Phys.*, 1956, **24**, 966-978.
4. R. A. Marcus, Electron-Transfer Reactions in Chemistry - Theory and Experiment, *Rev. Mod. Phys.*, 1993, **65**, 599-610.
5. P. F. Barbara, T. J. Meyer and M. A. Ratner, Contemporary Issues in Electron Transfer Research, *J. Phys. Chem.*, 1996, **100**, 13148-13168.
6. C. A. Angell, Formation of Glasses from Liquids and Biopolymers, *Science*, 1995, **267**, 1924-1935.

7. G. P. Wiederrecht, W. A. Svec and M. R. Wasielewski, Controlling the Adiabaticity of Electron-Transfer Reactions Using Nematic Liquid-Crystal Solvents, *J. Phys. Chem. B*, 1999, **103**, 1386-1389.

8. N. Liang, J. R. Miller and G. L. Closs, Temperature-independent long-range electron transfer reactions in the Marcus inverted region, *J. Am. Chem. Soc.*, 1990, **112**, 5353-5354.

9. J. Ulstrup and J. Jortner, The effect of intramolecular quantum modes on free energy relationships for electron transfer reactions, *J. Chem. Phys.*, 2008, **63**, 4358-4368.

10. M. Bixon and J. Jortner, Solvent relaxation dynamics and electron transfer, *Chem. Phys.*, 1993, **176**, 467-481.

11. M. Bixon and J. Jortner, in *Advances in Chemical Physics*, 1999, vol. 106, pp. 35-202.

12. G. R. Fleming, J. L. Martin and J. Breton, Rates of primary electron transfer in photosynthetic reaction centres and their mechanistic implications, *Nature*, 1988, **333**, 190-192.

13. M. Bixon and J. Jortner, Activationless and pseudoactivationless primary electron transfer in photosynthetic bacterial reaction centers, *Chem. Phys. Lett.*, 1989, **159**, 17-20.

14. H. B. Kim, N. Kitamura, Y. Kawanishi and S. Tazuke, Bell-shaped temperature dependence in quenching of excited $Ru(bpy)_3^{2+}$ by an organic acceptor, *J. Am. Chem. Soc.*, 1987, **109**, 2506-2508.

15. W. B. Davis, M. A. Ratner and M. R. Wasielewski, Conformational Gating of Long Distance Electron Transfer through Wire-like Bridges in Donor−Bridge−Acceptor Molecules, *J. Am. Chem. Soc.*, 2001, **123**, 7877-7886.

16. B. M. Hoffman and M. A. Ratner, Gated electron transfer: when are observed rates controlled by conformational interconversion?, *J. Am. Chem. Soc.*, 1987, **109**, 6237-6243.

17. H. A. Meylemans and N. H. Damrauer, Controlling Electron Transfer through the Manipulation of Structure and Ligand-Based Torsional Motions: A Computational Exploration of Ruthenium Donor−Acceptor Systems using Density Functional Theory, *Inorg. Chem.*, 2009, **48**, 11161-11175.

18. K. E. Spettel and N. H. Damrauer, Exploiting Conformational Dynamics of Structurally Tuned Aryl-Substituted Terpyridyl Ruthenium(II) Complexes to Inhibit Charge Recombination in Dye-Sensitized Solar Cells, *J. Phys. Chem. C*, 2016, **120**, 10815-10829.

19. D. V. Matyushov, Energetics of Electron-Transfer Reactions in Soft Condensed Media, *Accounts Chem. Res.*, 2007, **40**, 294-301.

20. M. M. Waskasi, G. Kodis, A. L. Moore, T. A. Moore, D. Gust and D. V. Matyushov, Marcus Bell-Shaped Electron Transfer Kinetics Observed in an Arrhenius Plot, *J. Am. Chem. Soc.*, 2016, **138**, 9251-9257.

21. M. M. Waskasi, M. D. Newton and D. V. Matyushov, Impact of Temperature and Non-Gaussian Statistics on Electron Transfer in Donor–Bridge–Acceptor Molecules, *J. Phys. Chem. B*, 2017, **121**, 2665-2676.

22. G. Lakhwani, A. Rao and R. H. Friend, Bimolecular Recombination in Organic Photovoltaics, *Annu. Rev. Phys. Chem.*, 2014, **65**, 557-581.

23. D. Gust, T. A. Moore and A. L. Moore, Solar Fuels via Artificial Photosynthesis, *Accounts Chem. Res.*, 2009, **42**, 1890-1898.

24. T. Mani, Molecular qubits based on photogenerated spin-correlated radical pairs for quantum sensing, *Chem. Phys. Rev.*, 2022, **3**, 021301.

25. S. M. Harvey and M. R. Wasielewski, Photogenerated Spin-Correlated Radical Pairs: From Photosynthetic Energy Transduction to Quantum Information Science, *J. Am. Chem. Soc.*, 2021, **143**, 15508-15529.

26. R. E. Blankenship, *Molecular mechanisms of photosynthesis*, John Wiley & Sons, Incorporated, Oxford, 2002.

27. E. Vauthey, Photoinduced Symmetry-Breaking Charge Separation, *Chemphyschem*, 2012, **13**, 2001-2011.

28. R. M. Young and M. R. Wasielewski, Mixed Electronic States in Molecular Dimers: Connecting Singlet Fission, Excimer Formation, and Symmetry-Breaking Charge Transfer, *Accounts Chem. Res.*, 2020, **53**, 1957-1968.

29. E. Sebastian and M. Hariharan, Symmetry-Breaking Charge Separation in Molecular Constructs for Efficient Light Energy Conversion, *ACS Energy Lett.*, 2022, **7**, 696-711.

30. L. Estergreen, A. R. Mencke, D. E. Cotton, N. V. Korovina, J. Michl, S. T. Roberts, M. E. Thompson and S. E. Bradforth, Controlling Symmetry Breaking Charge Transfer in BODIPY Pairs, *Accounts Chem. Res.*, 2022, **55**, 1561-1572.

31. N. Saki, T. Dinc and E. U. Akkaya, Excimer emission and energy transfer in cofacial boradiazaindacene (BODIPY) dimers built on a xanthene scaffold, *Tetrahedron*, 2006, **62**, 2721-2725.

32. A. C. Benniston, G. Copley, A. Harriman, D. Howgego, R. W. Harrington and W. Clegg, Cofacial Boron Dipyrromethene (Bodipy) Dimers: Synthesis, Charge Delocalization, and Exciton Coupling, *J. Org. Chem.*, 2010, **75**, 2018-2027.

33. M. A. H. Alamiry, A. C. Benniston, G. Copley, A. Harriman and D. Howgego, Intramolecular Excimer Formation for Covalently Linked Boron Dipyrromethene Dyes, *J. Phys. Chem. A*, 2011, **115**, 12111-12119.

34. J. H. Golden, L. Estergreen, T. Porter, A. C. Tadle, D. Sylvinson M. R, J. W. Facendola, C. P. Kubiak, S. E. Bradforth and M. E. Thompson, Symmetry-Breaking Charge Transfer in Boron Dipyridylmethene (DIPYR) Dimers, *ACS Appl. Energy Mater.*, 2018, **1**, 1083-1095.

35. I. J. Arroyo-Córdoba, R. Sola-Llano, N. Epelde-Elezcano, I. L. Arbeloa, V. Martínez-Martínez and E. Peña-Cabrera, Fully Functionalizable β, β' -BODIPY Dimer: Synthesis, Structure, and Photophysical Signatures, *J. Org. Chem.*, 2018, **83**, 10186-10196.

36. E. Sebastian and M. Hariharan, Null Exciton-Coupled Chromophoric Dimer Exhibits Symmetry-Breaking Charge Separation, *J. Am. Chem. Soc.*, 2021, **143**, 13769-13781.

37. Z. Li, Y. Liu, X. Hou, Z. Xu, C. Liu, F. Zhang and Z. Xie, The crystal structures, spectrometric, photodynamic properties and bioimaging of β-β linked Bodipy oligomers, *J. Lumin.*, 2019, **212**, 306-314.

38. X.-F. Zhang, BisBODIPY as PCT-based halogen free photosensitizers for highly efficient excited triplet state and singlet oxygen formation: Tuning the efficiency by different linking positions, *Dyes Pigm.*, 2017, **146**, 491-501.

39. F. Bergström, I. Mikhalyov, P. Hägglöf, R. Wortmann, T. Ny and L. B. Å. Johansson, Dimers of Dipyrrometheneboron Difluoride (BODIPY) with Light Spectroscopic Applications in Chemistry and Biology, *J. Am. Chem. Soc.*, 2002, **124**, 196-204.

40. I. H. M. van Stokkum, D. S. Larsen and R. van Grondelle, Global and target analysis of time-resolved spectra, *Biochim. Biophys. Acta Bioenerg.*, 2004, **1657**, 82-104.

41. J. T. Buck, A. M. Boudreau, A. DeCarmine, R. W. Wilson, J. Hampsey and T. Mani, Spin-Allowed Transitions Control the Formation of Triplet Excited States in Orthogonal Donor-Acceptor Dyads, *Chem*, 2019, **5**, 138-155.

42. H. vanWilligen, G. Jones and M. S. Farahat, Time-resolved EPR study of photoexcited triplet-state formation in electron-donor-substituted acridinium ions, *J. Phys. Chem.*, 1996, **100**, 3312-3316.

43. M. T. Colvin, A. B. Ricks, A. M. Scott, D. T. Co and M. R. Wasielewski, Intersystem Crossing Involving Strongly Spin Exchange-Coupled Radical Ion Pairs in Donor–bridge–Acceptor Molecules, *J. Phys. Chem. A*, 2012, **116**, 1923-1930.

44. Z. E. X. Dance, S. M. Mickley, T. M. Wilson, A. B. Ricks, A. M. Scott, M. A. Ratner and M. R. Wasielewski, Intersystem crossing mediated by photoinduced intramolecular charge transfer: Julolidine-anthracene molecules with perpendicular pi systems, *J. Phys. Chem. A*, 2008, **112**, 4194-4201.

45. Z. E. X. Dance, Q. X. Mi, D. W. McCamant, M. J. Ahrens, M. A. Ratner and M. R. Wasielewski, Time-resolved EPR studies of photogenerated radical ion pairs separated by p-phenylene oligomers and of triplet states resulting from charge recombination, *J. Phys. Chem. B*, 2006, **110**, 25163-25173.

46. N. K. Lee, S. Park, M.-H. Yoon, Z. H. Kim and S. K. Kim, Effect of ring torsion on intramolecular vibrational redistribution dynamics of 1,1′ -binaphthyl and 2,2′ -binaphthyl, *Phys. Chem. Chem. Phys.*, 2012, **14**, 840-848.

47. H. L. Kee, C. Kirmaier, L. Yu, P. Thamyongkit, W. J. Youngblood, M. E. Calder, L. Ramos, B. C. Noll, D. F. Bocian, W. R. Scheidt, R. R. Birge, J. S. Lindsey and D. Holten, Structural Control of the Photodynamics of Boron−Dipyrrin Complexes, *J. Phys. Chem. B*, 2005, **109**, 20433-20443.

48. M. K. Kuimova, G. Yahioglu, J. A. Levitt and K. Suhling, Molecular Rotor Measures Viscosity of Live Cells via Fluorescence Lifetime Imaging, *J. Am. Chem. Soc.*, 2008, **130**, 6672-6673.

49. P. Vath and M. B. Zimmt, A Spectroscopic Study of Solvent Reorganization Energy: Dependence on Temperature, Charge Transfer Distance, and the Type of Solute−Solvent Interactions, *J. Phys. Chem. A*, 2000, **104**, 2626-2633.

50. P. Vath, M. B. Zimmt, D. V. Matyushov and G. A. Voth, A Failure of Continuum Theory: Temperature Dependence of the Solvent Reorganization Energy of Electron Transfer in Highly Polar Solvents, *J. Phys. Chem. B*, 1999, **103**, 9130-9140.

Table of Contents (TOC) Entry